The role of metal ions in phosphate ester hydrolysis

Shina C. L. Kamerlin[a] and John Wilkie*[b]

Received 29th January 2007, Accepted 4th May 2007
First published as an Advance Article on the web 30th May 2007
DOI: 10.1039/b701274h

Many phosphatases make use of metal ions to aid catalysis of phosphate ester hydrolysis. Here, we investigate the impact of metal ions on the potential energy surface (PES), and hence the preferred reaction mechanism, for a simple model for hydrolysis of phosphate ester monoanions. We show that, while both associative ($A_N + D_N$) and dissociative ($D_N + A_N$) mechanisms are represented on the potential energy surfaces both in the presence and absence of metal ions, the $D_N + A_N$ process is favoured when there are no metal ions present and the $A_N + D_N$ process is favoured in the presence of two metal ions. A concerted (A_ND_N) process is also available in the presence of two metal ions, but proceeds *via* a high-energy transition state. In the presence of only a single metal ion the A_ND_N process is the most favoured, but still proceeds *via* a high-energy transition state. Thus, we conclude that metallo-enzyme phosphatases are likely to utilise an associative process, while those that function without metal ions may well follow a dissociative process.

Introduction

Importance of phosphate ester hydrolysis

Hydrolysis of phosphate esters is of crucial importance to biological systems, being involved in energy transduction, biosynthesis, control of secondary messengers and regulation of protein function. Inevitably, a wide range of enzymes has evolved to catalyse this deceptively simple reaction, operating *via* a range of different mechanisms and under a wide range of different conditions. Thus, there are enzymes that function in high pH and low pH, that utilise direct attack by water or employ an enzyme-derived nucleophile in a double displacement reaction, that employ metal ions in catalysis and others that do not. Phosphate ester hydrolysis has also become the focus of much effort in the design of artificial catalysts,[1–7] many of which draw inspiration from known enzyme structures.

Mechanisms for the hydrolysis of phosphate esters differs fundamentally from the mechanism for the hydrolysis of equivalent carboxylate esters on account of the availability of low-lying d-orbitals on the phosphorus atom. Thus, pentavalent phosphorus species are available as intermediates in the hydrolysis mechanism. As a result, hydrolysis may proceed *via* either a pentavalent (often described as "associative") or trivalent (described as "dissociative") intermediate. Alternatively, a concerted process, in which bond-making and bond-breaking occur in a single reaction step, passes through a single transition state structure without an intermediate (Scheme 1).

These three processes may be formally termed $A_N + D_N$, $D_N + A_N$ and A_ND_N, respectively, though the latter, concerted, process may also be regarded as either associative or dissociative, depending on the bond-orders at the transition state. In addition, our earlier work[8] suggested that there might also be equivalent non-inline processes for each of the mechanisms described above, for a total of eight distinct mechanisms. However, our work also suggested that the non-inline processes had broadly similar reaction barriers to their inline equivalents so, for the purpose of this paper, they have been ignored. The remaining four inline mechanisms can all be described on a More O'Ferrall–Jencks plot, Fig. 1, in which reactants are located at the lower right corner, products at the upper left. A dissociative process ($D_N + A_N$) would then proceed *via* the upper left region of the plot, whereas an associative process ($A_N + D_N$) would proceed *via* the lower right region. Concerted processes (A_ND_N) are often depicted as heading across the middle of the plot, but can pass though any part of the plot, being either associative or dissociative in character depending on the total bond orders for the making and breaking bonds at transition state. The key distinction for concerted processes is the absence of an intermediate (local minimum) along the reaction pathway.

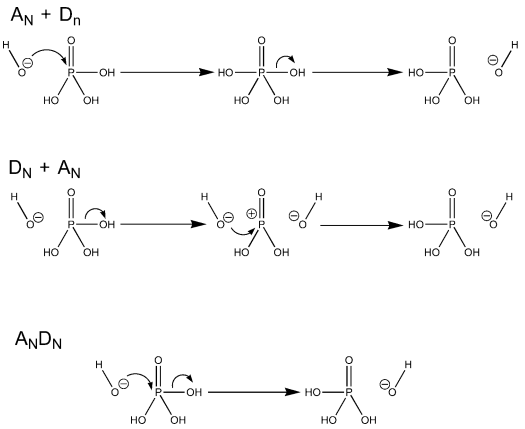

Scheme 1 $A_N + D_N$, $D_N + A_N$ and A_ND_N mechanisms.

Here we present 2-dimensional energy surfaces for the identity reaction involving water exchange on the phosphate monoanion as a model for phosphate ester hydrolysis. The dimensions of the plot represent formation of the P–O bond to the incoming nucleophile and breaking of the P–O bond to the leaving group.

[a]*University of Vienna, Institute of Biomolecular Structural Chemistry, Vienna, Austria. E-mail: l.kamerlin@gmx.at; Fax: +43 (0)1 4277 527 16; Tel: +43 (0)1 4277 527 90*
[b]*School of Chemistry, Birmingham University, Birmingham, UK. E-mail: j.wilkie@bham.ac.uk; Fax: +44 (0)121 414 4403; Tel: +44 (0)121 414 7189*

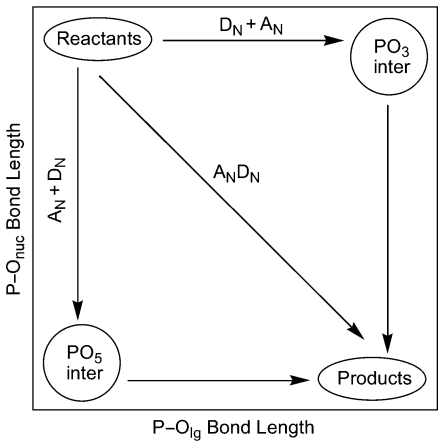

Fig. 1 More O'Ferrall–Jencks plot showing the routes across the potential energy surface followed by $A_N D_N$, $A_N + D_N$ and $D_N + A_N$ processes.

As these 2-dimensional surfaces are, in reality, simply projections of the full PES onto 2-dimensions, there are multiple points from the full surface corresponding to each individual point on our 2-dimensional surface; points with different coordinates that are not directly related to the bond-making and bond-breaking events of interest. Variation in these other coordinates adds noise to the 2D plots and can obscure key features of the potential energy surface. It is, therefore, essential to keep the number of additional coordinates to a minimum and to investigate multiple conformations corresponding to each point on the plot to ensure that the true lowest energy 2D plot is obtained. Thus by focusing on the water exchange reaction, we are able to avoid complications that may arise from variation in the orientation of the leaving group. Also, by exploiting an identity reaction, the potential energy surface will be symmetrical about the P–O_{nuc} : P–O_{lg} diagonal. A consequence of this symmetry is that any reaction pathway will cross this diagonal exactly once and thus by simply plotting the diagonal, the number of valid pathways across the surface can be identified simply from the number of valleys on the diagonal. This relationship between the diagonal and the 2D surface is not necessarily true for non-symmetrical systems.

These 2-dimensional potential energy surfaces allow us to determine which mechanisms are available to the systems under study and provide an indication of their relative barrier heights. In particular, we are interested in whether the presence of metal ions has an impact on the preferred mechanism.

Solution and enzyme-bound mechanisms

For monoesters in aqueous solution, hydrolysis has generally been accepted as following a largely dissociative mechanism,[9–11] citing large negative β_{lg} and little participation of the nucleophile in the rate-limiting step as evidence to support this.[12] It was also assumed for quite some time that enzyme catalysis would somehow drive the mechanism towards a more associative process in keeping with the compact nature of most enzyme active sites.[13–15] More recently, there has been extensive experimental investigation into the catalytic mechanisms of a number of phosphatases alongside many computational studies of various model systems. It is clear from these results that a number of different reaction mechanisms are employed by various enzymes. Thus, KIE results have been used to postulate a dissociative transition state for various phosphotyrosine phosphatases (PTPases).[16] Alkaline phosphatase has been shown to exhibit a large negative β_{lg} for both phosphate and sulfate substrates (both -0.76)[17,18] compared with -1.23 for phosphate ester hydrolysis in solution[12]—evidence that has been used to support a dissociative mechanism for this enzyme also.[17,18] However, a similarly large β_{lg} (-1.38)[19] has be shown for dinuclear Co catalysts, for which KIEs indicate a concerted associative mechanism.[7] Unfortunately, KIEs for alkaline phosphatase are around 1 for a wide range of substrates, indicating a non-chemical rate-limiting step.[20]

In addition, perusal of the literature reveals that a variety of mechanisms have been proposed for metallo-phosphatases and their dinuclear biomimetic equivalents.[7,17,21–24] Essentially, these mechanisms can be boiled down to two, differing in the arrangement of the metal ions with respect to nucleophile and leaving group (Scheme 2). Generally, these mechanisms have been proposed on the basis of X-ray crystal structures and type 1 (Scheme 2) has been applied to purple-acid phosphatase, Ser/Thr protein phosphatases and many small dinuclear catalysts,[7,17,22] whereas type 2 has been applied to alkaline phosphatase and inositol monophosphatase.[21,23–24] Recent crystal structures of enzymes with bound transition state analogues have been used to argue in favour of a dissociative mechanism for phosphoserine protease (PSP),[25] which does not utilise metal ions, and for an associative mechanism for the metallo-enzyme, β-phosphoglucomutase,[26] though interpretation of the latter structure has lead to some controversy.[27,28]

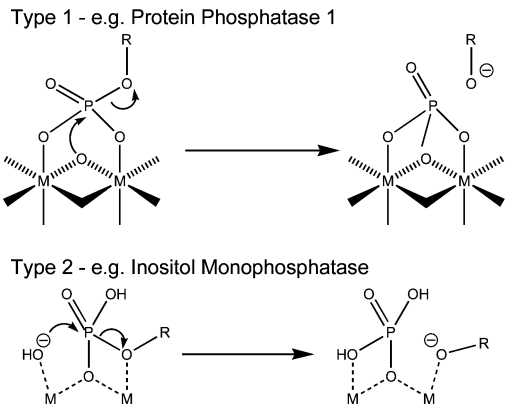

Scheme 2 Proposed reaction mechanisms for protein phosphatase 1 (type 1) and inositol monophosphatase (type 2), both shown as concerted $A_N D_N$ processes.

Phosphate ester hydrolysis has also been extensively investigated using a variety of theoretical methods and model systems.[29–40] Unfortunately, most previous work considers only a single possible mechanism for the particular system under consideration. Furthermore, it is rare to find the same system considered across several studies, thus it is difficult to come to any mechanistic conclusion based on computational work alone. Where both associative and dissociative mechanisms have been considered,[29] dissociative transition states have been determined in the absence of a nucleophile, so the two mechanisms are not directly comparable. Thus both $A_N + D_N$[29,31–33] and $D_N + A_N$[30] mechanisms have been proposed for the solution reaction based on computational results. Computational studies of the reaction mechanism in

enzymes have been similarly inconclusive as, again, methods such as coordinate-following with QM/MM systems require an assumption of the type of mechanism in advance. Thus $D_N + A_N$ pathways have been claimed for phosphotyrosine protein phosphatases (PTPases)[34,35,39] in addition to both dissociative[36] and associative[37] $A_N D_N$ pathways[36] as well as an $A_N + D_N$ pathway for monoanions.[38] It should be noted that the latter study identified a $D_N + A_N$ pathway for dianions.[38] Only one other study[40] has effectively considered the possibility of a variety of different mechanisms for any given system and, in common with the results presented here, that paper also determined 2-dimensional potential energy surfaces for phosphate ester hydrolysis. Klähn[40] *et al.* consider non-symmetrical reactions in which leaving group ≠ nucleophile and so, barrier heights cannot be compared directly with those here. In addition, they consider dianions, and do not look at the role of metal ions coordinating to both nucleophile and leaving group. However, Klähn's results show that simple dianions prefer associative pathways with no clear intermediates. Pyrophosphate trianions, on the other hand, show both associative and dissociative concerted ($A_N D_N$) mechanisms with the dissociative mechanism preferred. The only consideration of metal ions lies in the inclusion of a single ion, binding to a non-bridging oxygen in a triphosphate. This is a model for ATP hydrolysis, and so represents a rather different system from those considered here.

Methodology

Model reaction

Water exchange involving the phosphate monoanion ($H_2PO_4^-$) has been taken as the model system for this study, though, as there is both experimental and computational evidence to support the possibility of proton transfer during the reaction, proton positions have been allowed to optimise during the calculations (Scheme 3). As a result, this same model is able to able to describe the hydroxide exchange on neutral phosphate. From a consideration of pK_a, the reaction might be expected to involve the phosphate dianion (HPO_4^{2-}) in aqueous solution; involvement of the dianion in gas-phase calculations is both unrepresentative and leads to problems with optimisation. In aqueous solution, phosphate oxygen atoms participate in a number of hydrogen bonds, serving to attenuate substantially any negative charge; similarly while bound in an enzyme active site phosphate groups are frequently in close association with positively charged amino acids. It has also been argued that the hydrolytic reaction may well prefer the monoanion.[7] Thus, it is appropriate to reduce the charge on the phosphate group in a gas-phase calculation. In addition, optimisation of strongly negatively-charged species frequently leads to positive energies for occupied orbitals leading to unbound electrons. Trial calculations showed that the system described here (H_3PO_4/OH^- or $H_2PO_4^-/H_2O$) gave stable optimisation both in the presence and absence of metal ions.

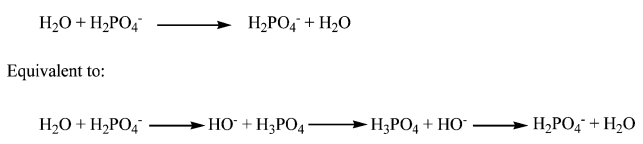

Scheme 3 Model reaction considered in this work.

As Mg^{2+} ions do not possess any valence electrons, do not show redox behaviour in this context and are found in a number of phosphatase enzymes, they represent the metal ion of choice for this work.

In order to compare associative mechanisms directly with the corresponding dissociative mechanism, 2-dimensional potential energy surfaces (PES) have been determined with specified P–O_{lg} and P–O_{nuc} distances as the two dimensions, all other geometrical variables (including proton positions) being allowed to optimise, so adding energy contours to the More O'Ferrall–Jencks plot, Fig. 1. By considering dissociative reactions in the presence of the nucleophile in this way, the number and nature of the atoms involved remains constant and barrier heights taken from the PES for the various processes are now directly comparable.

As a consequence of considering a symmetrical reaction (nucleophile and leaving group are identical), the PES for the reaction should also be symmetrical about the diagonal (P–O_{lg} = P–O_{nuc}) of the plot. Furthermore, a consequence of this symmetry is that any reaction pathway for hydroxide exchange must itself be symmetrical about the diagonal and is therefore constrained to cross the diagonal only once. Thus a simple one-dimensional plot of the diagonal of the PES will reveal the number of distinct reaction pathways available for the system—each minimum on this one-dimensional plot will correspond to either a transition state or an intermediate along a distinct reaction pathway. A frequency calculation on each of these points will distinguish between transition states on concerted pathways and intermediates on stepwise pathways. Determination of the full PES will be required to identify transition states for stepwise processes along with reactant and product complexes, which will then allow determination of reaction barriers for the various pathways.

Solvation has been simulated by means of correction to SCF energy, rather than by inclusion of explicit solvent molecules, as the latter approach introduces additional degrees of freedom into the system, both complicating the 2-dimensional surfaces and substantially increasing computer time. Furthermore, introduction of loosely bound species renders transition state determination impossible on account of the large number of soft vibrations brought about by the weak non-bonding interactions. Thus, it is also not possible to introduce counter charges to offset the charge of the Mg^{2+} ions without also preventing transition state determination in their presence.

Computation

All calculations have been performed using Gaussian 03[41] and the 6-31++G(d,p)[42] basis set thus placing diffuse and polarisation functions on all atoms in the system. Second order Møller–Plessett pertubation[43] has been applied to Hartree–Fock optimisations and frequency calculations whilst DFT calculations have made use of a combination of Barone's 1-parameter modified Perdew–Wang 91 exchange functional[44] and the Perdew–Wang 91 correlation functional (MPW1PW91).[45] Discussions are based primarily on results obtained using DFT, but attention is drawn to any situation in which MP2-based calculations gave different results. Solvation effects have been simulated by applying a PCM[46] correction to key DFT stationary points with Gaussian 03. The PCM calculations

made use of the UFF model rather than the default UAO model as a number of transition states also included some degree of proton transfer.

In the absence of metal ions, starting points for the diagonal of the PES are quite simple to determine. When $P–O_{lg} = P–O_{nuc}$ (as required for the diagonal), the structures possess C_{2v} symmetry (considering only the heavy atoms) so starting points were constructed, constraining both $P–O_{lg}$ and $P–O_{nuc}$ to the specified distance at 0.2 Å intervals and adding hydrogen atoms maintain C_{2v} symmetry. Structures were subjected to free optimisation with only $P–O_{lg}$ and $P–O_{nuc}$ constrained to their specified values.

Adding two metal ions to the system complicates matters. It is possible to obtain structures with both C_2 and C_{2v} symmetry for the same values of $P–O_{lg}$ and $P–O_{nuc}$, these structures differing only in the positioning of the metal ions. Thus, for short P–O distances at least, starting points were generated with each of the two possible symmetries and optimised with only $P–O_{lg}$ and $P–O_{nuc}$ constrained. (At long P–O distances, the C_2 structures optimised to C_{2v} analogues so additional starting points were not required). In cases where optimisation from C_2 and C_{2v} starting points gave different optimised results, the lower energy result has been taken for the plot.

With only a single metal ion, all structures are asymmetric so the metal ion was initially placed 2.0 Å from one hydroxide ion, designated (somewhat artificially) as the nucleophile.

Starting points for the full PES were generated in a similar manner but with $P–O_{lg}$ and $P–O_{nuc}$ specified and constrained independently. In this case, points are taken at 0.1 Å intervals.

Accurate determination of stationary points started from the nearest constrained optimised structure on the PES and subjected it to a fully unconstrained optimisation (also no symmetry constraints). Transition states and local minima were verified by means of a frequency calculation on the optimised geometry at the same level of theory as was used for the geometry optimisation.

Results and discussion

Phosphate ester hydrolysis in the absence of metal ions

Calculations with P–O bond distances constrained to values greater than 3.6 Å failed to converge in SCF, but it is clear from both the diagonal (Fig. 2a) and full PES (Fig. 2b) that there are two distinct reaction paths—one with a minimum at $P–O_{lg} = P–O_{nuc}$ ≈ 1.8 Å, the other with a minimum, both P–O distances >3.4 Å.

Unconstrained optimisation of the points closest to each minimum produced structures for a pentavalent $A_N + D_N$ intermediate (Fig. 3a) with P–O bond lengths of 1.77 Å and a trivalent $D_N + A_N$ intermediate with P–O bond lengths of 3.42 Å (Fig. 3b). Both intermediates show C_{2v} symmetry. As optimisation of the reactant complex (Fig. 3c) showed the reaction to involve both a water molecule and the phosphate monoanion, both pathways involve a proton transfer, concerted with either P–O bond breaking or making. In the case of the $A_N + D_N$ pathway, this proton is transferred from the nucleophile to one of the phosphate oxygen atoms along a pre-existing hydrogen bond, whereas in the $D_N + A_N$ example, proton transfer occurs from a phosphate oxygen atom to the departing leaving group.

An approximate transition state could be identified from the 2-dimensional PES for the $A_N + D_N$ process: this led to a fully optimised transition state with $P–O_{nuc} = 2.18$ Å and $P–O_{lg} = 1.71$ Å (Fig. 4), resulting in a barrier height of 38.4 kcal mol^{-1}. Though the 2-dimensional PES is suggestive of a $D_N + A_N$ transition state with $P–O_{lg} \approx 2.2$ Å and $P–O_{nuc} \approx 3.4$ Å, unconstrained optimisation resulted in an increase in the value of $P–O_{nuc}$, leading eventually to SCF failure. Thus, it was not possible to obtain an optimised $D_N + A_N$ transition state in the presence of the nucleophile. The apparent shallow saddle point on the PES is an artefact arising from the fact that the 2-dimensional PES is merely a projection of the full PES into two dimensions. As a consequence of this projection, there are a large number of structures that can correspond to each point on the surface (*i.e.*, they retain the specified values for $P–O_{lg}$ and $P–O_{nuc}$ but other geometrical parameters can vary. Though these variations generally result in small changes to the energy, they can produce the appearance of spurious stationary points that are not maintained under full optimisation). Thus, as the PES becomes quite flat with increasing P–O distance at the extremes of the plot, these small local variations can have an impact on the appearance of the plot.

There seems to be a ridge developing at $P–O_{lg} = 2.0$ Å and $P–O_{nuc} > 3.4$ Å, with the true transition state lying somewhere on the ridge, but with a large value of $P–O_{nuc}$. It is clear, however, that the barrier for the $D_N + A_N$ pathway, at around 28 kcal mol^{-1}, is lower than that of the $A_N + D_N$ pathway. For comparison, the dissociative reaction pathway (D_N step only) for $H_2PO_4^-$ was also calculated in the absence of nucleophile. This resulted in the transition state

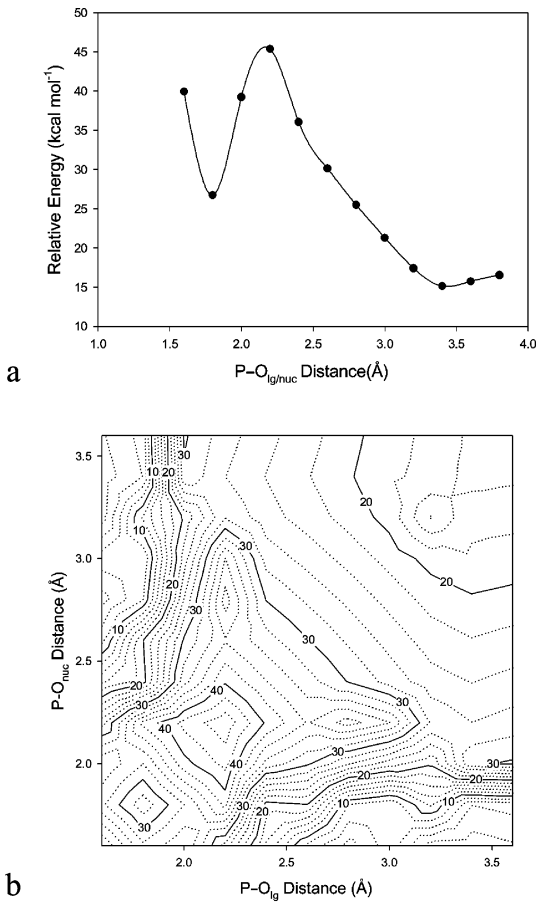

Fig. 2 DFT-Calculated PES in the absence of metal ions. (a) Diagonal; (b) 2-dimensional PES.

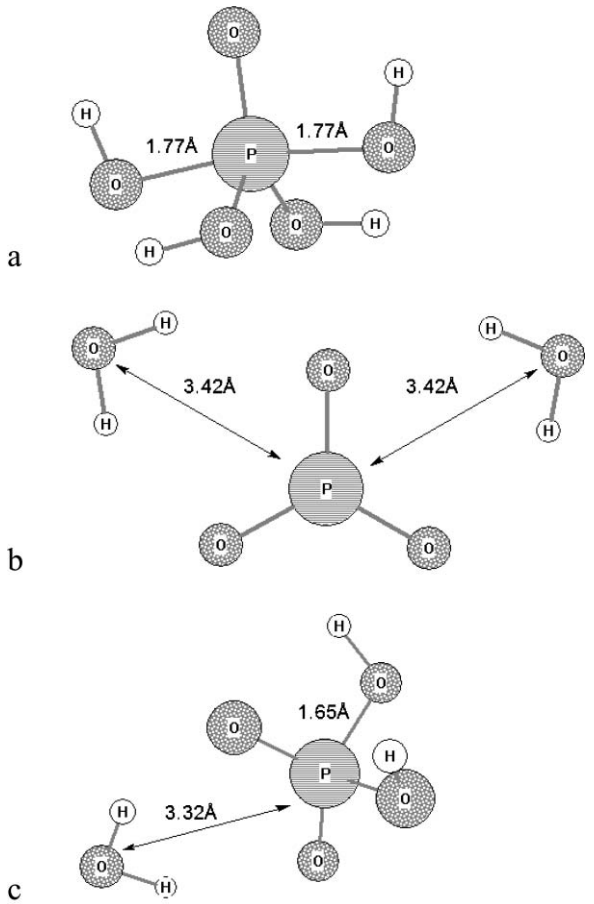

Fig. 3 DFT-Optimised structures in the absence of metal ions for (a) associative intermediate, (b) dissociative intermediate, (c) reactant complex.

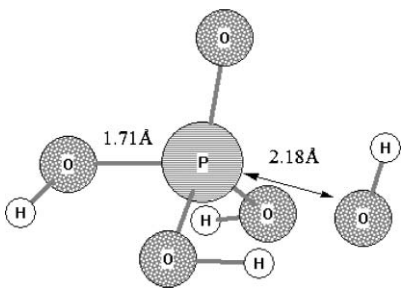

Fig. 4 DFT-Optimised transition state for an $A_N + D_N$ mechanism in the absence of metal ions.

(Fig. 5) with P–O_{lg} = 2.08 Å and a reaction barrier of 34.19 kcal mol^{-1}, suggesting either a small degree of stabilisation of the transition state or a destabilisation of the reactant by the presence of the nucleophile.

MP2 calculations give a remarkably similar picture to that obtained *via* DFT, with only minimal differences in geometry and barrier heights. Calculations employing MP2 were slightly less effective at combating SCF problems at longer fixed P–O distances while taking up more memory and CPU-time.

Applying a PCM correction to the key stationary points in order to simulate solvation of the system produces a quantitative change in the relative barrier heights for the two mechanisms but

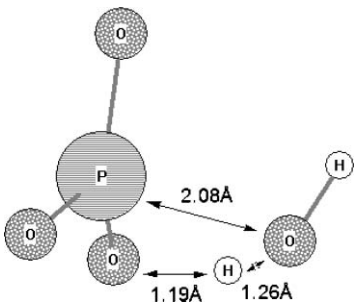

Fig. 5 DFT-Optimised transition state for P–O bond dissociation in the absence of both metal ions and nucleophile.

no change in the preferred mechanism. Though transition states could not be determined for the dissociative $D_N + A_N$ process, taking the point closest to the ridge on Fig. 2b, suggests that the barrier for this process changes by less than 1 kcal mol^{-1} whereas the barrier height for the associative process is reduced by a little over 2 kcal mol^{-1}. By far the largest effect is the destabilisation of the dissociative intermediate by 9 kcal mol^{-1}

Table 1 shows a summary of the key geometric parameters and energies of the stationary points.

Phosphate ester hydrolysis in the presence of two metal ions

The diagonal of the potential energy surface in the presence of metal ions clearly shows at least two distinct reaction paths when using DFT (Fig. 6a). These two paths correspond to the stepwise $A_N + D_N$ and $D_N + A_N$ pathways described for the system without metal ions. As in the previous case, SCF convergence problems were experienced at long fixed P–O separations limiting the extent to which the 2-dimensional PES could be plotted with the result that the $D_N + A_N$ intermediate lies beyond the reach of the plot (Fig. 6b).

The $A_N + D_N$ intermediate (Fig. 7a) shows only C_2 symmetry, with a rotational axis running from the P-atom to the O-atom that does not interact with either metal ion. There is no mirror plane of symmetry. This contrasts topologically with the equivalent TS in the absence of metal ions, which possesses a mirror plane of symmetry and so has C_{2v} symmetry. The presence of metal ions extends P–O_{lg} and P–O_{nuc} in the intermediate to 1.82 Å (compared with 1.77 Å in their absence). The symmetry of this pathway differs therefore from that of both pathways observed in the absence of metal ions.

Examination of the full 2D-PES (Fig. 6b) reveals an $A_N + D_N$ transition state which optimises to P–O_{nuc} = 2.29 Å, P–O_{lg} = 1.75 Å (Fig. 8) and a barrier-height of 24.53 kcal mol^{-1}. Comparing this structure with the optimised reactant complex (P–O_{nuc} = 3.51 Å, P–O_{lg} = 1.71 Å, Fig. 7b) shows very little change in the length of the breaking bond but a dramatic shortening of the making bond, consistent with an associative process. Significantly, the metal–metal distance also shortens dramatically as the reaction proceeds (Table 2).

Though both the diagonal and full PES suggested the presence of a $D_N + A_N$ intermediate, SCF failure for P–O_{nuc} > 3.6 Å prevented optimisation of both the intermediate and transition state. The shape of the full PES suggests however that the barrier height for this process is likely to be in excess of 40 kcal mol^{-1}, substantially greater than for the $A_N + D_N$ process.

Table 1 Energies and key geometric parameters of stationary points for the model reaction in the absence of metal ions. Geometries and energies for stationary points in the absence of metal ions

	(a) DFT					(b) MP2				
	Reactant complex	$A_N + D_N$ transition state	$A_N + D_N$ intermediate	$D_N + A_N$ transition state	$D_N + A_N$ intermediate	Reactant complex	$A_N + D_N$ transition state	$A_N + D_N$ intermediate	$D_N + A_N$ transition state	$D_N + A_N$ intermediate
P–O_{nuc}/Å	3.32	2.18	1.77	>3.6	3.43	3.36	2.22	1.77	>3.4	3.45
P–O_{lg}/Å	1.65	1.71	1.77	≈2.2	3.43	1.67	1.72	1.77	≈2.3	3.45
Total energy/Hartree	−719.99478	−719.93358	−719.95277	N/D	−719.97071	−718.64141	−718.57604	−718.59651	N/D	−718.62270
Relative energy/kcal mol^{-1}	0	+38.40	+26.36	≈+28	+15.10	0	+41.02	+28.17	≈+28	+11.73
PCM energy/kcal mol^{-1}	0	+36.08	+24.81	≈+30	+24.36	—	—	—	—	—

Fig. 6 DFT-Calculated PES in the presence of two metal ions. (a) Diagonal; (b) 2-dimensional PES.

Fig. 7 DFT-Optimised structures in the presence of two metal ions for (a) associative intermediate; (b) reactant complex.

The diagonal of the PES from HF calculations with MP2 (Fig. 9a) shows a curious profile. There is an abrupt change in gradient at P–O = 2.1 Å and a third path with a shallow valley on the diagonal at P–O = 2.3 Å. Though this third pathway does not show up on the full PES, with contours at 2 kcal mol^{-1} intervals (Fig. 9b); increasing the resolution of the 2-dimensional PES to

Table 2 Energies and key geometric parameters of stationary points in the presence of two metal ions. Geometries and energies for stationary points in the presence of two metal ions

	(a) DFT				(b) MP2			
	Reactant complex	$A_N + D_N$ transition state	$A_N + D_N$ intermediate	$A_N D_N$ transition state	Reactant complex	$A_N + D_N$ transition state	$A_N + D_N$ intermediate	$A_N D_N$ transition state
P–O_{nuc}/Å	3.51	2.29	1.82	2.27	3.52	2.28	1.83	2.43
P–O_{lg}/Å	1.71	1.75	1.82	2.27	1.72	1.76	1.83	2.43
Mg–Mg/Å	7.92	6.18	5.59	8.07	8.01	6.13	5.66	8.45
Total energy/Hartree	−1118.98739	−1118.94829	−1118.96645	−1118.91749	−1116.80863	−1116.77088	−1116.78847	−1116.80863
Relative energy/kcal mol^{-1}	0	+24.53	+13.14	+43.86	0	+23.69	+12.65	+42.80
PCM energy/kcal mol^{-1}	0	+14.89	+2.69	+41.05	—	—	—	—

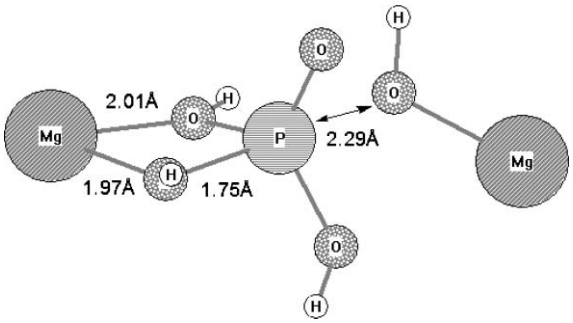

Fig. 8 DFT-Optimised transition state for an $A_N + D_N$ mechanism in the presence of two metal ions.

include points at 0.05 Å intervals and reducing the contour interval to 0.04 kcal mol^{-1} reveals a saddle point for both MP2 and DFT calculations (Fig. 9c,d). Unconstrained optimisation results in a 1st order transition state corresponding to a concerted $A_N D_N$ pathway in which the P–O_{nuc} bond is formed at the same time as the P–O_{lg} bond is broken. Both P–O_{nuc} and P–O_{lg} = 2.27 Å and the transition state as a whole has C_{2v} symmetry (Fig. 10). The barrier height for this process is 43.86 kcal mol^{-1}, almost 20 kcal mol^{-1} greater than the $A_N + D_N$ process. This $A_N D_N$ process also differs from the $A_N + D_N$ process in that the metal ion separation increases as the reaction proceeds to the transition state.

The change in symmetry between the $A_N D_N$ transition state and $A_N + D_N$ intermediate accounts for the abrupt change in the gradient at P–O = 2.1 Å. This point highlights the intersection of two distinct surfaces: one based around C_2 symmetrical structures and the other around C_{2v} symmetrical structures. For P–O < 2.1 Å, the C_2 surface has lower energy whereas for P–O > 2.1 Å the C_{2v} surface has lower energy and the abrupt change in gradient occurs as the favoured structures switch from one surface to the other.

Adding Mg^{2+} ions inevitably changes the overall charge of the system, and here we see an impact on the overall mechanism: as both leaving group and nucleophile are coordinated by metal ions, there is no need for proton transfer between phosphate and nucleophile/leaving group, contributing acid-catalysis to the reaction. Rather the metal ions can be thought to act to some extent as Lewis acid catalysts.

Once again, including solvation has an impact on the individual barrier heights, but not to the extent of changing the preferred mechanism. The preferred $A_N + D_N$ mechanism is stabilised to the greatest extent, solvation reducing the barrier to 14.89 kcal mol^{-1} while the $A_N D_N$ process is stabilised to a lesser extent (barrier now 41.05 kcal mol^{-1}). The dissociative intermediate is destabilised to such an extent that its energy is raised above the notional "transition state" for this process. As the relative energy of the dissociative intermediate is now some 95 kcal mol^{-1} higher than the reactant complex, the $D_N + A_N$ process is no longer observed.

A summary of key geometric variables and energies of stationary points for both MP2 and DFT calculations are presented in Table 2.

One metal ion

When the reaction occurring in the presence of a single metal ion is considered, the 2D-PES is no longer symmetrical about the diagonal and the assumption regarding the separation of pathways

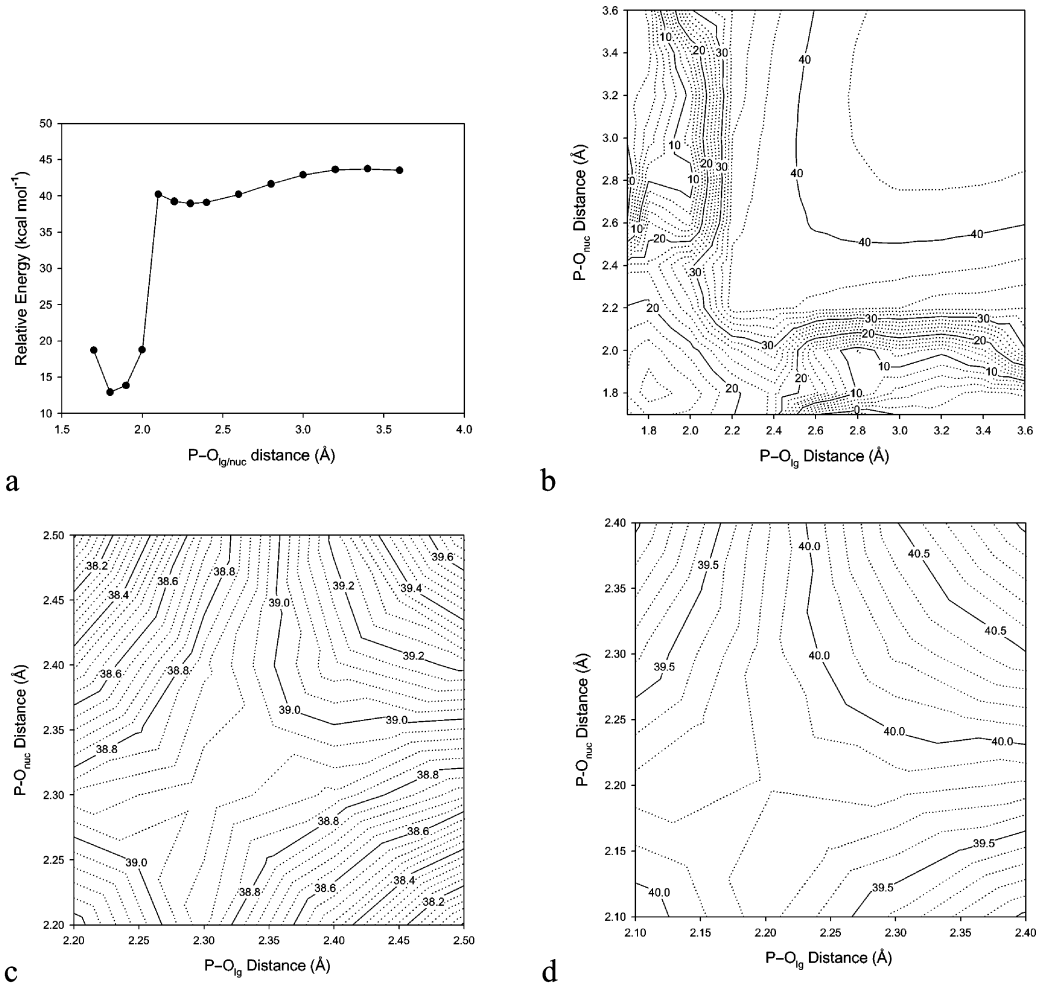

Fig. 9 PES in the presence of two metal ions. (a) Diagonal of the MP2-calculated PES; (b) 2-dimensional MP2-calculated PES; (c) high-resolution 2-dimensional MP2-calculated PES covering the region around the $A_N D_N$ transition state; (d) high-resolution DFT-calculated plot covering the same region.

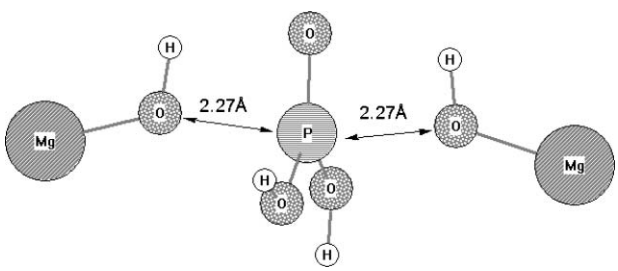

Fig. 10 DFT-Optimised transition state for an $A_N D_N$ mechanism in the presence of two metal ions.

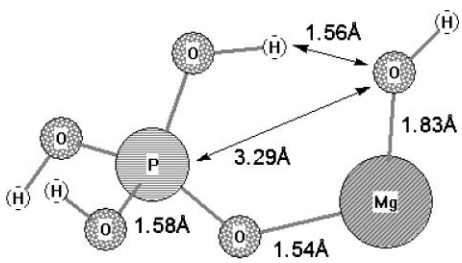

Fig. 11 DFT-Optimised reactant complex with one metal ion showing the relative positions of metal ion, nucleophile and leaving group.

along the diagonal does not necessarily hold true in this case. For the purposes of this discussion, the metal ion is considered to be interacting with the nucleophilic oxygen (Fig. 11) though it could just as easily be regarded as interacting with the oxygen of the leaving group by simply exchanging the labels on the 2D-PES plot.

It is clear from the PES that there is no $A_N + D_N$ intermediate in this case (Fig. 12), rather the reaction proceeds *via* a concerted $A_N D_N$ pathway. Optimisation of this transition state gave an asymmetric TS with P–O_{nuc} = 2.09 Å and P–O_{lg} = 2.28 Å (Fig. 13). A proton has been spontaneously transferred from the phosphate to the leaving group in this structure. The barrier height for this process is 41.07 kcal mol^{-1}, remarkably similar to that for the $A_N D_N$ process with two metal ions. Frequency and IRC calculations both confirmed that this transition state is a first order transition state, with the transition vector corresponding to making and breaking correct P–O bonds. A composite calculation involving following the IRC for a small number (6) of steps in each direction followed by unconstrained energy optimisation also resulted in reactant

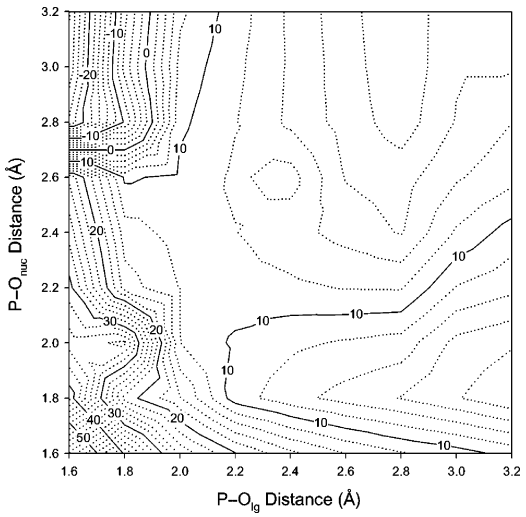

Fig. 12 2-Dimensional DFT calculated PES in the presence of one metal ion.

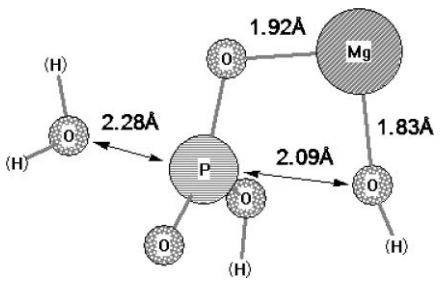

Fig. 13 DFT-Optimised transition state for an A_ND_N mechanism in the presence of one metal ion.

and product structures rather than an associative intermediate, so we can be confident that the $A_N + D_N$ pathway does not exist for this system with only a single metal ion present.

No $D_N + A_N$ intermediate can be observed on the PES though, once again, problems with SCF at long P–O distances for making and breaking bonds may have prevented the plot extending sufficiently. However, it is clear from the plot that should a dissociative intermediate exist, the barrier height along the pathway towards it will be greater than that for the concerted A_ND_N pathway. Energies and geometries of key stationary points are given in Table 3.

Approximate transition states and intermediate for the $D_N + A_N$ were determined from the 2-dimensional potential energy surface (Fig. 12) and along with reactant, product and A_ND_N transition state, had a PCM correction applied to simulate solvation. By far the most dramatic effect of the solvent was to almost abolish the thermodynamic component of the reaction. Following expectations, the barrier height for the A_ND_N process was also reduced. By way of contrast, barrier heights for the disfavoured $D_N + A_N$ process were increased by a small amount (approximately 3 kcal mol^{-1} for the bond-breaking event) as was observed for two metal ions. The dissociative intermediate was destabilised sufficiently to abolish the transition state for the subsequent bond-breaking event and as its energy was now some 50 kcal mol^{-1} above that of the reactant complex, it is safe to say that the $D_N + A_N$ process will not be followed for this reaction.

As this reaction is no longer fully symmetrical, there is a potentially a thermodynamic contribution to this reaction, which is not present in the other two cases. As it is somewhat arbitrary to assign the reactants and products as described above, the reverse assignment could apply equally well and would give a barrier height of just 11.5 kcal mol^{-1} before consideration of solvation. However, once solvation is taken into account, the thermodynamic contribution is just 2.8 kcal mol^{-1} and thus forward and reverse barriers are comparable at around 35 kcal mol^{-1}.

Conclusions

Potential energy surfaces for the hydroxide exchange reaction in all three cases (no metal ions, two metal ions, one metal ion) show the existence of multiple reaction pathways converging on the same reactant and products. However, though multiple pathways were present for each set of conditions, the individual pathways show rather different barrier heights and in each case, a single pathway would be preferred. The identity of this preferred reaction pathway depends on the number of metal ions present. Applying a PCM correction to simulate the effects of solvent changes the numerical values of barrier heights but does not lead to any change in preferred mechanism for any of the processes. With either one or two metal ions present, the dissociative intermediate is sufficiently destabilised relative to the transition state for conversion to product, to abolish the pathway.

Transition states optimised both in the presence of metal ions and their absence showed the metal ions serving principally to bring about a change in reaction mechanism. In their absence, the preferred mechanism is a stepwise $D_N + A_N$ process whereas, in the presence of metal ions, a stepwise $A_N + D_N$ process is preferred. This change is achieved by both increasing the barrier height of the $D_N + A_N$ process and decreasing the barrier height for the $A_N + D_N$ process. There appears to be only a small change in barrier height for the preferred process in each circumstance (from 28 kcal mol^{-1} without metal ions to 24 kcal mol^{-1} with

Table 3 DFT energies and key geometric parameters of stationary points in the presence of one metal ion. Geometries and energies for stationary points in the presence of one metal ion

(a) DFT

	Reactant complex	A_ND_N transition state	Product complex
P–O$_{nuc}$/Å	3.29	2.09	1.83
P–O$_{lg}$/Å	1.58	2.28	3.34
Total energy/Hartree	−918.04698	−917.98153	−917.99986
Relative energy/kcal mol^{-1}	0	+41.07	+29.57
PCM energy/kcal mol^{-1}	0	+34.88	+2.83

metal ions—though the "without metal ions" case should be regarded as an upper limit only). Though the presence of metal ions allowed a concerted A_ND_N reaction pathway with a C_{2v} symmetrical transition state, this pathway has a much larger barrier height than the geometrically-similar stepwise pathway and so is unlikely to contribute in any way to the overall reaction. Allowing for solvation leads to a more dramatic change in barrier height, reducing the barrier for the preferred $A_N + D_N$ process in the presence of metal ions to 14.89 kcal mol^{-1} while having only a minimal effect on the barrier in the absence of metal ions.

Curiously, the single-metal-ion case shows the largest barrier height of the three examples. The presence of a single metal ion is able to hinder either loss of leaving group or approach of nucleophile (depending on which it interacts with) without producing the activation of an $A_N + D_N$ process as is achieved in the presence of two metal ions. Indeed only the concerted A_ND_N process could be observed, occurring with a similar barrier height to that with two metal ions, the equivalent stepwise process being completely absent. Even inclusion of solvation does not bring the barrier height below that of the other two examples.

These results are consistent with experimental evidence regarding the mechanisms for phosphate ester hydrolysis. Though most experimental procedures are unable to distinguish concerted from stepwise mechanisms in this context, there is evidence to support a dissociative hydrolysis mechanism in aqueous solution (corresponding to our model in the absence of metal ions). Similarly, enzymes that do not employ metal ions in catalysis have quite open active sites (as exemplified by the protein tyrosine phosphatases) and can quite easily accommodate transition states and intermediates forming a dissociative mechanism. In contrast, a number of mechanisms have been proposed for metallo-enzyme phosphatases, most of which involve an associative mechanism (again, not usually distinguishing between stepwise and concerted processes). In particular, a number of metallo-enzyme phosphatases, such as inositol monophosphatase, completely enclose their substrates in the active site, an approach that would be inconsistent with a dissociative mechanism. Examination of metal–metal distances in the X-ray crystal structures of various metallo-enzyme phosphatases shows the values obtained for our $A_N + D_N$ pathway coming close those seen in the crystal structures. In particular, this process shows a steady decrease in metal ion separation as the reaction proceeds to the intermediate and this structure shows the closest comparison to the experimental structures (Table 4). Of the enzymes listed, both alkaline phosphatase[23] and inositol monophosphatase[24] have been argued to utilise a mechanism similar to the one identified here,[21] namely with one metal ion assisting attack of the nucleophile, the other aiding departure of the leaving group (Scheme 2). However, an alternative mechanism has been proposed for both Ser/Thr protein phosphatases[22] and certain organometallic catalysts[7] in which the nucleophile is a μ-bridging hydroxide, and so bound to both metal ions. In this mechanism, leaving group departure is aided by an enzyme-derived general acid and it is, therefore, not surprising that these systems show a rather shorter metal–ion separation. Configurations corresponding to transition state-like structures for this mechanism proved not to be stable for our simple model systems—on optimisation, the leaving group and metal ions would rearrange themselves to interact with each other, giving one of the transition state structures described earlier. Of course, this observation does not mean that such a mechanism is not viable, as both the enzyme and organometallic systems have additional functional groups and structural constraints not present in our system.

Table 4 Metal–metal distances in representative metallo-phosphatase crystal structures and key stationary points for the model reaction in the presence of two metal ions. Purple acid phosphatase and protein phosphatase 1 have both been proposed to follow a type 1 (Scheme 2) mechanism while alkaline phosphatase and inositol monophosphatase have both been proposed to follow a type 2 mechanism

System	Metal–metal distance/Å
Protein phosphatase 1 (1fjm)	3.27
Purple acid phosphatase (1kbp)	3.32
Inositol monophosphatase (1imd)	4.04
Alkaline phosphatase (1alk)	4.12
Calculated reactant complex (DFT)	7.92
Calculated $A_N + D_N$ intermediate (DFT)	5.59
Calculated $A_N + D_N$ transition state (DFT)	6.18
Calculated A_ND_N transition state (DFT)	8.07

Interestingly, though a large number of phosphatases employing two metal ions in catalysis and those that do not involve metal ions have been identified, there are currently no examples of true phosphatases employing a single metal ion in catalysis. The results shown here suggest a rationale for this observation, namely that whereas the presence of two metal ions leads to a reduction in barrier height compared with the reaction in the absence, inclusion of only a single metal ion leads to an increase in barrier height.

References

1 F. Aguilar-Perez, P. Gomez-Tagle, E. Collado-Fregoso and A. K. Yatsimirsky, *Inorg. Chem.*, 2006, **45**, 9502–9517.
2 S. Parimala and M. Kandaswany, *Transition Met. Chem.*, 2004, **29**, 35–41.
3 M. Padovani, N. H. Williams and P. Wyman, *J. Phys. Org. Chem.*, 2004, **17**, 472–477.
4 F. Verge, C. Lebrun, M. Fontecave and S. Menage, *Inorg. Chem.*, 2003, **42**, 499–507.
5 C. Vichard and T. A. Kaden, *Inorg. Chim. Acta*, 2004, **357**, 2285–2293.
6 N. H. Williams, A.-M. Lebuis and J. Chin, *J. Am. Chem. Soc.*, 1999, **121**, 3341–3348.
7 T. Humphrey, M. Forconi, N. H. Williams and A. C. Hengge, *J. Am. Chem. Soc.*, 2004, **126**, 11864–11860.
8 J. Wilkie and D. Gani, *J. Chem. Soc., Perkin Trans. 2*, 1996, 783–787.
9 M. Henchman, A. A. Viggiano, J. F. Paulson, A. Freedman and J. Wormhoudt, *J. Am. Chem. Soc.*, 1985, **107**, 1453–1455.
10 J. M. Friedman, S. Freeman and J. R. Knowles, *J. Am. Chem. Soc.*, 1988, **110**, 1268–1275.
11 D. Herschlag and W. P. Jencks, *J. Am. Chem. Soc.*, 1989, **111**, 7579–7586.
12 A. J. Kirby and A. G. Varvoglis, *J. Am. Chem. Soc.*, 1967, **89**, 415–423.
13 A. Hasset, W. Blatter and J. R. Knowles, *Biochemistry*, 1982, **21**, 6335–6340.
14 D. Herschlag and W. P. Jencks, *Biochemistry*, 1990, **29**, 5172–5179.
15 A. S. Mildvan, *Proteins*, 1997, **24**, 401–416.
16 A. C. Hengge, *FEBS Lett.*, 2001, **501**, 99–102.
17 I. Nikolic-Hughes, D. C. Rees and D. Herschlag, *J. Am. Chem. Soc.*, 2004, **126**, 11814–11819.
18 F. Hollfelder and D. Herschlag, *Biochemistry*, 1995, **34**, 12255–12264.
19 N. H. Williams, W. Cheung and J. Chin, *J. Am. Chem. Soc.*, 1998, **120**, 8079–8087.
20 A. C. Hengge, W. A. Edens and H. Elsing, *J. Am. Chem. Soc.*, 1994, **116**, 5045–5049.
21 D. Gani and J. Wilkie, *Struct. Bonding*, 1997, **89**, 133–175.
22 M.-P. Egloff, P. T. W. Cohen, P. Reinemer and D. Barford, *J. Mol. Biol.*, 1995, **254**, 942–959.
23 E. E. Kim and H. W. Wyckoff, *J. Mol. Biol.*, 1991, **218**, 449–464.

24 R. Bone, L. Frank, J. P. Springer, S. J. Pollack, S. A. Osborne, J. R. Atack, M. R. Knowles, G. McAllister, C. I. Ragan, H. B. Broughton, R. Baker and S. R. Fletcher, *Biochemistry*, 1994, **33**, 9460–9467.
25 W. Wang, H. S. Cho, R. Kim, J. Jancarik, H. Yokota, H. H. Nguyen, I. V. Grigoriev, D. E. Wemmer and S.-H. Kim, *J. Mol. Biol.*, 2002, **319**, 421–431.
26 S. D. Lahiri, G. Zhang, D. Dunaway-Mariano and K. N. Allen, *Science*, 2003, **299**, 2067–2071.
27 G. M. Blackburn, N. H. Williams, S. J. Gamblin and S. J. Smerdon, *Science*, 2003, **301**, 1184c.
28 K. N. Allen and D. Dunaway-Mariano, *Science*, 2003, **301**, 1184d.
29 G. M. Arantes and H. Chaimovich, *J. Phys. Chem. A*, 2005, **109**, 5625–5635.
30 J. M. Mercero, P. Barrett, C. W. Lam, J. E. Fowler, J. M. Ugalde and L. G. Pedersen, *J. Comput. Chem.*, 2000, **21**, 43–51.
31 Y. Liu, B. A. Gregersen, A. Hengge and D. M. York, *Biochemistry*, 2006, **45**, 10043–10053.
32 Y. Liu, B. A. Gregersen, X. Lopez and D. M. York, *J. Phys. Chem. B*, 2006, **109**, 19987–20003.
33 X. Lopez, A. Dejaegere, F. Leclerc, D. M. York and M. Karplus, *J. Phys. Chem. B*, 2006, **110**, 11525–11539.
34 K. Kolmodin, P. Nordlund and J. Aqvist, *Proteins*, 1999, **36**, 370–379.
35 K. Kolmodin and J. Aqvist, *Int. J. Quantum Chem.*, 1999, **73**, 147–159.
36 P. G. Czyryca and A. C. Hengge, *Biochim. Biophys. Acta*, 2001, **1547**, 235–253.
37 C. Alhambra, L. Wu, Z.-Y. Zhang and J. Gao, *J. Am. Chem. Soc.*, 1998, **120**, 3858–3866.
38 D. Asthagiri, V. Dillet, T. Liu, L. Noodleman, R. L. Van Etten and D. Bashford, *J. Am. Chem. Soc.*, 2002, **145**, 10225–10235.
39 B. L. Grigorenko, A. V. Rogov and A. V. Nemukhin, *J. Phys. Chem. B*, 2006, **110**, 4407–4412.
40 M. Klahn, E. Rosta and A. Warshel, *J. Am. Chem. Soc.*, 2006, **128**, 15310–15323.
41 M. J. Frisch, G. W. Trucks, H. B. Schlegel, G. E. Scuseria, M. A. Robb, J. R. Cheeseman, J. A. Montgomery, Jr., T. Vreven, K. N. Kudin, J. C. Burant, J. M. Millam, S. S. Iyengar, J. Tomasi, V. Barone, B. Mennucci, M. Cossi, G. Scalmani, N. Rega, G. A. Petersson, H. Nakatsuji, M. Hada, M. Ehara, K. Toyota, R. Fukuda, J. Hasegawa, M. Ishida, T. Nakajima, Y. Honda, O. Kitao, H. Nakai, M. Klene, X. Li, J. E. Knox, H. P. Hratchian, J. B. Cross, V. Bakken, C. Adamo, J. Jaramillo, R. Gomperts, R. E. Stratmann, O. Yazyev, A. J. Austin, R. Cammi, C. Pomelli, J. Ochterski, P. Y. Ayala, K. Morokuma, G. A. Voth, P. Salvador, J. J. Dannenberg, V. G. Zakrzewski, S. Dapprich, A. D. Daniels, M. C. Strain, O. Farkas, D. K. Malick, A. D. Rabuck, K. Raghavachari, J. B. Foresman, J. V. Ortiz, Q. Cui, A. G. Baboul, S. Clifford, J. Cioslowski, B. B. Stefanov, G. Liu, A. Liashenko, P. Piskorz, I. Komaromi, R. L. Martin, D. J. Fox, T. Keith, M. A. Al-Laham, C. Y. Peng, A. Nanayakkara, M. Challacombe, P. M. W. Gill, B. G. Johnson, W. Chen, M. W. Wong, C. Gonzalez and J. A. Pople, *GAUSSIAN 03 (Revision C.02)*, Gaussian, Inc., Wallingford, CT, 2004.
42 R. Ditchfield, W. J. Hehre and J. A. Pople, *J. Chem. Phys.*, 1971, **54**, 724–728.
43 M. J. Frisch, M. Head-Gordon and J. A. Pople, *Chem. Phys. Lett.*, 1990, **166**, 275–280.
44 C. Adamo and V. Barone, *J. Chem. Phys.*, 1998, **108**, 664–675.
45 J. P. Perdew, K. Burke and Y. Wang, *Phys. Rev. B*, 1996, **54**, 16533–16539.
46 E. Cances, B. Mennucci and J. Tomasi, *J. Chem. Phys.*, 1997, **107**, 3032–3041.

